Strength of strained two-phase mixtures: Application to rapid creep and stress amplification in subduction zone mélange

Adam Beall[1], Åke Fagereng[1] and Susan Ellis[2]

[1]School of Earth & Ocean Sciences, Cardiff University, Cardiff, CF10 3AT, UK.

[2]GNS Science, 1 Fairway Dr., Avalon, Lower Hutt 5010, New Zealand

Corresponding author: Adam Beall (bealla1@cardiff.ac.uk)

Key Points:

- 2D mélange shear zones require ≥ 50% weak matrix to accommodate steady creep at low stress, otherwise force chains lead to jamming.
- Transient creep (slow slip) events may occur in mélange with ≤ 50% weak matrix during temporary absence of force chains
- Stress amplification, and potentially tremor, occurs even in steadily creeping mélange

This article has been accepted for publication and undergone full peer review but has not been through the copyediting, typesetting, pagination and proofreading process which may lead to differences between this version and the Version of Record. Please cite this article as doi: 10.1029/2018GL081252

Abstract

Aseismic creep may occur by distributed deformation in mélange shear zones comprising weak matrix and stronger clast materials. Slow slip events (SSEs) or steady tectonic displacement can be distributed over < 100 m thick shear zones if weak matrix controls bulk shear zone deformation. We use 2D numerical models to quantify the rheology of moderately strained (shear-strain < 1.75) mélange for various volumetric proportions of competent clasts. Mélange deformation with < 50% clasts is matrix dominated and can accommodate steady creep. At higher clast proportions mélange viscosity increases more than 10-fold after small strains, because strong clasts interact and form force chains. Clast shear stress is amplified above the imposed shear stress, by a factor of < 14 where force chains develop. SSEs may occur due to a temporary absence of force chains, while localized regions of high shear stress generate coincident fracturing and potentially tremor events.

Plain Language Summary

Some subduction shear zones creep without generating large earthquakes. It is unclear which deformation process at depth allows this creep to occur. We compute numerical models to explore whether creep is promoted by having a particular proportion of weak materials within subduction fault zones, which typically consist of mixtures (‘mélanges’) of weak and strong components. We demonstrate that in a mélange that consists of < 50% weak minerals, forces are concentrated into ‘force chains’ of strong materials when the mélange is slightly deformed, resulting in an overall strength which is much greater than previously predicted. Subduction zone creep events therefore occur in mélanges either with a high proportion of weak minerals, or in the temporary absence of such force concentrations. Swarms of very small earthquakes are often associated with creep events, which likely require failure of the stronger mélange materials. We show that large forces are generated in the strong materials, plausibly leading to this failure, even when the overall mélange is very weak.

1. Introduction

Subduction megathrust displacement may be localized along discrete millimeter-thick faults or distributed over 1-100 m thick shear zones (Rowe et al., 2013). Distributed shear is promoted when the subduction zone interface is a tabular zone, a subduction mélange, where strong clasts are embedded within a matrix of weaker, typically clay-rich, material (Fagereng & Den Hartog, 2017; Shreve & Cloos, 1986). Mélange rheology may be approximated by bulk deformation of the matrix, if the volumetric ratio ϕ = (clast volume)/(total volume) is small (Grigull et al., 2012). Above a critical ϕ, deformation may be accommodated by brittle faulting of strong blocks and localized strain of the intervening matrix (Fagereng & Sibson, 2010). Such localized slip can occur transiently when matrix shear pathways are blocked by interlocking clasts (e.g. Webber et al., 2018), so that a subset of clasts become load-bearing 'force chains' in a process called 'jamming' (Cates et al., 1998). It is unclear what this critical ϕ is; estimates vary from $\phi \approx 0.45$ (Roscoe, 1952) to ≥ 0.8 (Handy, 1994).

Slow slip events (SSEs) are transient episodes of aseismic slip lasting from days to years, at rates of $\sim 0.1 - 1$ m yr^{-1}, significantly faster than time-averaged plate velocities (Dragert et al., 2001; Miyazaki et al., 2006; Schwartz & Rokosky, 2007; Wallace & Beavan, 2010). These slip rates correspond to transient bulk strain-rates ($\dot{\epsilon}_{xy}$) of $10^{-11} - 10^{-10}$ s^{-1} (and higher localized strain-rates) if shear is distributed across a 100 m thick tabular zone. SSEs may be explained by rate-and-state variable friction, assuming a fine-tuned combination of frictional properties for a planar fault surface active at low effective normal stress (Rubin, 2008). We explore an alternative, that SSEs are episodes of relatively rapid, distributed visco-brittle deformation (Lavier et al., 2013, Kano et al., 2018). Estimates for subduction thrust interface shear stress are on the order of 10 MPa (Davis et al., 1983; Duarte et al., 2015; Gao & Wang, 2014; Richardson & Coblentz, 1994), while SSEs are modulated by small tidal stresses (Rubenstein et al., 2008; Hawthorne and Rubin, 2010), implying only kPa order stress drops. SSEs within subduction interface shear zones are therefore only reconcilable with deformation of weak matrix minerals (Fagereng et al., 2014), implying either low ϕ or a temporary absence of force chains.

Relatively deep SSEs are commonly accompanied by an increased activity of tectonically activated, low frequency seismic signals known as 'tremor' (Obara et al., 2004; Rogers &

Dragert, 2003). This 'episodic tremor and slow slip' implies simultaneous creep and frictional sliding within a shear zone below the seismogenic zone. In a model where creep and fracture occur within a compositionally heterogeneous mélange, inference of low shear stress implies that frictional failure of the strong mélange components occurs due to near-lithostatic pore-pressure (Sibson, 2013) or transiently elevated elastic stress (Hayman & Lavier, 2014). We explore an alternative where localized high-stress clast deformation occurs within a low bulk stress state mélange, as a result of stress amplification in localized load-bearing regions, but without causing jamming of the shear zone.

We use generalized models to systematically examine how mélange jamming and stress amplification depend on ϕ and strain. Newtonian rheologies are assumed, such that results can be non-dimensionalized and applied to the variety of depths, effective stress-states and rock compositions that SSEs occur in. Subduction zone mélange matrix commonly consists of mixtures of frictional and soluble minerals (e.g. muscovite and quartz), deforming by rate-limiting pressure-solution once frictional sliding occurs (Bos et al., 2000; Fagereng and Den Hartog, 2017; Den Hartog and Spiers, 2014; Niemeijer & Spiers, 2007). Pressure-solution creep is approximated by a Newtonian rheology, which can also be used for a simplified representation of relatively rigid clasts. As fracturing is not explicitly modelled, calculated maximum stresses and mélange strengths are upper limits that can be used to predict whether fracturing is likely to occur under specific modelled conditions.

2. Model Setup

To accommodate bulk SSE strain-rates of $10^{-11} - 10^{-10}\mathrm{s}^{-1}$ under 10 MPa driving stress, a shear zone would need an effective viscosity η_{eff} (satisfying Eq. 1, for shear stress τ) in the range $10^{16} - 10^{17}$ Pa s.

$$\tau = 2\eta_{eff}\dot{\epsilon}_{xy} \quad (1)$$

'Effective viscosity' implies that this viscosity approximates processes other than monomineralic creep; e.g. brittle failure (discussed by Fullsack, 1995), complex polymineralic deformation (Niemeijer & Spiers, 2007), or heterogeneous deformation of contrasting rock domains (the focus of this paper). We calculate η_{eff} for a generalized two-phase mixture, examining how the relative velocities of the shear zone walls, and the shear zone's internal stress and strain-rate distributions, respond to an imposed τ and evolving clast network during progressive finite shear strain.

We use 2D numerical models (Fig. 1) to calculate incompressible linear viscous flow of mélange for a variety of ϕ (0.3, 0.4, 0.5, 0.57 and 0.64) and ratios of matrix to clast viscosity η_m/η_c (10^{-4}, 10^{-3}, 10^{-2} and 10^{-1}), forming a set of 20 'reference' models. These viscosity contrasts reflect contrasting temperature-dependences of deformation in a range of minerals; e.g. at temperatures of < 400°C wet feldspar is extremely strong (Rybacki et al., 2006), while serpentine is very weak (Hilairet et al., 2007) so that $\eta_m/\eta_c < 10^{-4}$; however, at higher temperatures this viscosity ratio will change towards 1 as feldspar weakens significantly. Similar relations can be found for many material pairs. The reference model domain is 4 m long and 1 m wide and starts with clast long-axes $\pm$30° to the horizontal walls. 'Additional' models explore extended parameter space. Sensitivity to shear zone thickness is explored by 'thin' end-member models with 4m x 0.5m domains for $\phi = 0.64$, and 'thick' end-members with 4m x 2m domains for $\phi = 0.5$ and $\phi = 0.64$. To test whether the initial sub-horizontal clast orientation reduces jamming potential, models with initially random clast orientations (horizontal to sub-vertical clast long-axes) are explored for $\phi = 0.64$. Each of these sensitivity tests covers the same η_m/η_c range as the reference models, forming a set of 16 additional models. Models are strained to $\epsilon_{xy} = 1.75$ (engineering shear-strain of 3.5), the smallest ϵ_{xy} at which every model appears to have reached a quasi-steady-state η_{eff}.

The particle-in-cell finite-element code Underworld (Moresi et al., 2007) is used to solve the velocity (v_x,v_y) and pressure (mean normal stress) fields, as well as the associated strain-rate and deviatoric stress tensors. Periodic boundary conditions are used, where their influence is reduced by the large model aspect ratio. The top wall assumes $v_y = 0$ and a constant bulk shear stress $\tau = \tau_0$, allowing for variable bulk mélange strain-rate through time. The bottom wall assumes $v_x = v_y = 0$. All models have 0.39 cm x 0.39 cm elements.

All results can be non-dimensionalized and rescaled, because the viscous flow (Stokes) equations with a Newtonian rheology are linear. Model stress is expressed as a non-dimensionalized ratio to τ_0. η_{eff} is time-dependent and calculated as 0.5 τ_0 w v_{top}^{-1}, where v_{top} is the average horizontal velocity on the top wall and w is the model thickness (0.5, 1 or 2 m). Mélange strength is expressed as the non-dimensional ratio η_{eff}/η_m. Length scales can be expressed as a non-dimensional ratio to either the shear-zone thickness w or the long-axis length of the largest clast L_{clast} (0.84 m in all the models).

Models begin with randomly positioned clasts, in order to avoid artificial clast alignment (Fig. 1). Clasts are initially separated by ≥ 2 cm (> 5 elements), to ensure they are resolved as separate bodies. Though deformation may reduce this separation to one element, a particle volume-weighting integration scheme is used in Underworld to approximately resolve intervening matrix. Clast long-axis lengths vary from 24 cm to $L_{clast} = 84$ cm. This range represents the smallest clast influencing the shear-zone scale flow field and the largest clast in the shear zone, respectively. All clasts have a 1:3 aspect ratio, mimicking the lens-shaped clasts typically observed in mélanges (Bachmann et al., 2009; Fagereng & Sibson, 2010; Grigull et al., 2012). Jamming occurs when ϕ is close to the maximum particle packing density (Krieger & Dougherty, 1959). Compared to circular clasts, the chosen diamond shape can pack more densely and may jam at a higher ϕ.

Clast sizes follow a power law size distribution, $N \propto r^{-D}$, where *N* is the number of clasts with length > *r* and *D* is a fractal parameter. *D* is set to 1.9, reflecting measured clast size distributions in exhumed mélanges dominated by ductile, rather than brittle, deformation structures (Fagereng, 2011a). As fractal clast-size distributions have a similar appearance at any scale, the models are scale-invariant and their geometry can be scaled, e.g. scaling the reference model with $w = 1$ m up to $w = 100$ m results in a 400 m × 100 m shear zone containing blocks with $L_{clast} = 84$ m. Viscosity and stress measurements are non-dimensionalized and therefore independent of scaling. Models are therefore applicable to the full spectrum of behavior that occurs in a ~100 m thick subduction megathrust assuming the clast-size distribution holds to this scale (e.g. Fagereng, 2011a; Grigull et al., 2012).

Fig. 1a shows a typical progression in mélange geometry with increasing strain for $\eta_m/\eta_c = 10^{-4}$ and $\phi = 0.5$. After $\epsilon_{xy} = 1.75$, clast interaction has led to formation of force chains (Fig. 1a; Movie S1) and strengthening from $\eta_{eff} = 4.3\eta_m$ to $49.5\eta_m$. Clast interaction and stress changes depend on ϕ and w (Fig. 1b).

3. Calculated Effective Viscosity

The effective viscosity η_{eff} is a function of η_m/η_c, ϕ and ϵ_{xy} (Fig. 2a). At $\epsilon_{xy} = 0$, η_{eff} can be approximated by the microphysical suspension model of Roscoe (1952) and the empirical mixing law of Ji (2004). The Roscoe model only approximates our results for $\eta_m/\eta_c = 10^{-3}$

and 10^{-4}, as it assumes $\eta_c \rightarrow \infty$, whereas Ji's model approximates all cases. The Reuss (discussed by Ji, 2004) and Handy ('interconnected-weak-layer', 1994) models are typically considered as lower bounds, and predict significantly lower η_{eff} than our models.

Jamming is quantified by η_{eff}/η_m (>>1 indicates jamming), calculated as the maximum η_{eff} occurring over $\epsilon_{xy} \leq 1.75$. η_{eff} increases with strain, though to varying degrees. For $w = 1$ m and $\eta_m/\eta_c = 10^{-4}$, η_{eff}/η_m only increases by ~30% with increasing strain for $\phi = 0.3$ and 0.4, so that the strain-independent mixing laws are a good approximation (Fig. 2a). For $0.5 \leq \phi \leq 0.64$, significant strengthening to $47 \leq \eta_{eff}/\eta_m \leq 307$ occurs as force chains develop, a much higher bulk strength than in mixing laws ignoring jamming. Jamming for $\phi \geq 0.5$ is evident in the dependence of η_{eff}/η_m on η_c (similarity to 'clast supported' trend, Fig. 2b) and occurs because simple shear requires solid body rotation, which is difficult at high ϕ without clast deformation (e.g. Fig. 1; Movies S1 and S3).

Roscoe (1952) proposed a microphysical suspension model incorporating clast interaction (Fig. 2a), which predicts significant strengthening as ϕ approaches a critical packing volume and approximates our calculated η_{eff} for $\eta_m/\eta_c = 10^{-3}$ and 10^{-4}. The Voigt model is considered an upper bound (discussed by Ji, 2004), but predicts significantly greater η_{eff} for jammed mélange than our models (Fig. 1a). The initial orientation of the clasts has a negligible impact on the degree of strengthening at $\epsilon_{xy} = 1.75$ (Fig. 2a, red circle), contrary to the emphasis in previous studies (e.g. Treagus, 2002). This is because, at least for a relatively high $\phi = 0.64$, clasts can jam while remaining sub-horizontal (Fig. 1).

η_{eff} of mélange with $\phi = 0.64$, $w = 1$ m and $\eta_m/\eta_c = 10^{-4}$ has lower and upper bounds (over $\epsilon_{xy} \leq 1.75$) of $\eta_{eff}/\eta_m = 6.8$ and 171.9 respectively, so that η_{eff} is a factor of 39 larger when the mélange is jammed, compared to unjammed. This factor reduces to 6.4x and 1.8x for $\eta_m/\eta_c = 10^{-3}$ and 10^{-2} respectively (Fig. 2b). As this low factor for $\eta_m/\eta_c = 10^{-2}$ is identical when $w = 0.5$ m, η_{eff} variation in this case does not appear to increase further with increased jamming. Significant η_{eff} variations with strain are therefore unlikely to be explained by jamming of mélange with $\leq 10^2$ order viscosity contrast and Newtonian rheology. The variation of η_{eff} with strain may be reduced in nature, as jammed mélange is dominated by clast deformation, potentially involving cataclastic flow not modelled here.

The thickness was changed to thin and thick end-members of 0.5 m and 2 m, respectively, in order to examine the influence of *w* on η_{eff}. The thin end-member model further promotes jamming, increasing η_{eff}/η_m to 1881 at high strain (Fig. 2a, square). This significant contrast in η_{eff} between models with $w = 1$ m (1.2 L_{clast}) and 0.5 m (0.6 L_{clast}) indicates that shear zones with thickness $w < 1.2\ L_{clast}$ have an increased jamming tendency.

Models with $w = 2$ m, have η_{eff} similar to the reference models ($w = 1$ m) at $\epsilon_{xy} = 0$ and $\phi = 0.5$ and 0.64. Thickening the shear zone beyond $w = 1.2\ L_{clast}$ therefore has little impact on flow in the absence of clast interaction. At high strain, the larger *w* is highly effective at mitigating jamming for $\phi = 0.5$ (Figs. 1 and 2; Movie S2), resulting in $\eta_{eff} = 7\eta_m$ instead of $47\eta_m$ for $\eta_m/\eta_c = 10^{-4}$. This mitigation is negligible for $w = 2$ m and $\phi = 0.64$, as η_{eff}/η_m still strengthens to 172.

A force chain network spans the entire model width when $w = 2$ m and $\phi = 0.64$ (Movie S4), unlike the single dominating force chains in models with $w \leq 1$ m (Fig. 1). The longest force chain has a length of $\sim 1.7L_{clast}$, which appears to be a characteristic maximum length that can be observed in the models with $w = 2$ m ($2.4L_{clast}$), but is longer than the shear zone thickness of models with $w \leq 1$. Individual force chains appear to buckle and reorganize; however, the overall force chain network still transmits stress across the shear zone sufficiently for jamming.

4. Stress Amplification

The maximum 2D shear stress at a point, $\tau_{max} = (\sigma_1 - \sigma_2)/2$ (for maximum and minimum principal compressive stresses σ_1 and σ_2), is calculated for the matrix and clast regions separately. τ_{max} is calculated on every particle, except those in elements containing clast interfaces, and interpolated onto the mesh using inverse distance weighting. The particle-in-cell finite element method can result in overestimated τ_{max} close to clast edges (Deubelbeiss and Kaus, 2008). To avoid these local overshoots, the 95th percentile of τ_{max} is calculated (τ_{95}), avoiding clast edges and conservatively measuring localized high stress regions spanning clasts (Fig. 1). τ_{95} for each model run is averaged over $1.25 \leq \epsilon_{xy} \leq 1.75$. The amplification of clast stress above the imposed bulk stress τ_0 is significant for all models,

with $3.9 \leq \tau_{95}/\tau_0 \leq 5.4$ for $\eta_m/\eta_c = 10^{-2}$ and $6.8 \leq \tau_{95}/\tau_0 \leq 13.4$ for $\eta_m/\eta_c = 10^{-4}$ (Fig. 3a). As the analytical solution for stress amplification in a single clast is $2.67\tau_0$ (3:1 long to short axis ratio; Schmid & Podladchikov, 2003), clast interaction has a significant impact on the mélange stress state.

Stress amplification predominately occurs within force chains, which are high stress pathways subparallel to σ_1. Force chains form when simple shear becomes difficult without clast deformation. It follows that the highest clast stress amplification occurs when the force chains and jamming are most prominent, tested by plotting clast stress amplification against η_{eff}/η_m (Fig. 3a). Models with $\phi = 0.3$ actually have higher τ_{95} than $\phi = 0.4$ for the initial clast distributions used, because stress is amplified in clasts colliding with the shear zone walls, irrespective of ϕ. τ_{95} controlled by such colliding clasts can be relatively high, $\tau_{95}/\tau_0 = 5.4$ and 9.5 for $\eta_m/\eta_c = 10^{-3}$ and 10^{-4} respectively, demonstrating that jamming is not necessarily a prerequisite for significant localized amplification.

τ_{95} increases for $\phi = 0.5$ and 0.57, relative to lower ϕ, because jamming concentrates stress into force chains. This increased jamming is also reflected by a marked increase in η_{eff}/η_m as ϕ increases to ≥ 0.5 (Fig. 3a). Stress amplification decreases, however, for $\phi = 0.64$ (Fig. 3a). The thin end-member model involves similar or less stress amplification than the unjammed models. This is because of an increased number of force chains, distributing stress among a greater area of clast material. This is quantified by the standard deviation of τ_{max} (Fig. 3a), which follows a similar trend to stress amplification.

In contrast to the clast stress states, the matrix shear stress (measured as τ_{95}), reduces with increasing jamming (Fig 3b), such that there is actually reduction below the background stress at $\phi \geq 0.5$. The highest matrix stress amplification, which occurs for the model with the lowest clast/matrix ratio ($\phi = 0.3$), peaks at $1.36\tau_0$ and corresponds to narrow high strain-rate regions between clasts (Fig. 1).

5. Fracturing at Low Stress

Fracture and frictional sliding of clast and matrix materials occur in nature and are candidates for generating tremor (Behr et al., 2018; Chestler and Creager, 2017; Fagereng and Sibson, 2010; Fagereng et al., 2011). Tremor occurs at depths of < 40 km (e.g. Nankai and Cascadia;

Schwartz & Rokosky, 2007), requiring low effective friction coefficients, $\mu' = \mu(1 - f_p)$, for friction coefficient μ and ratio of pore-fluid pressure to lithostatic pressure f_p, of $\mu' \sim 0.03$ (Sibson, 2014). Matrix phyllosilicates and clays typically have $0.1 < \mu < 0.5$, (Byerlee, 1978; Saffer and Marone, 2003) indicating moderate to high overpressures of $0.7 \leq f_p \leq 0.94$. Clasts are likely to have a higher $\mu \approx 0.6$, following Byerlee (1978), requiring near lithostatic pore-pressure of $f_p = 0.95$. While near-lithostatic pore-pressure is plausible along some parts of a subduction zone interface, it is difficult to envisage this condition being reached widely enough to explain all incidences of slow slip and tremor (e.g. Nankai is inferred to have $f_p \sim 0.75$; Saffer and Tobin, 2011). Clast stress amplification potentially reduces the need for extreme fluid overpressures to explain local and transient fracturing or frictional sliding. The models are used to predict the onset of brittle/frictional failure. To calculate the stress field after failure, further iterations of a non-linear solution are required (Fullsack, 1995), which is beyond the aims of the current study.

Tensile fractures in clasts within exhumed mélanges are commonly interpreted to have required near-lithostatic fluid pressure to allow fracture within otherwise ductilely deforming shear zones (Byrne and Fisher, 1990; Fagereng et al., 2011; Ujiie et al., 2018). Furthermore, geophysical observations indicate that Low Frequency Earthquakes (LFEs, considered the constituents of tremor) occur by shear failure within dominantly creeping active subduction thrusts (Ide et al., 2007b; Chestler and Creager, 2017). Frictional failure can be modelled by the Coulomb criterion for shear failure along well-orientated planes (Eq. 2) and a simplified Hoek-Brown criterion for tensile fracture (Eq. 3), expressed in terms of τ_{max} and depth z (approximating mean stress by lithostatic pressure);

$$\tau_{max} = \frac{\mathrm{C} + \rho g z\left(1 - f_p\right)\mu}{\sqrt{1 + \mu^2}} \quad (2)$$

$$\tau_{max} = \frac{C}{m} + \rho g z\left(1 - f_p\right) \quad (3)$$

for cohesion $C = 50$ MPa and $\mu = 0.6$ (following Byerlee's law), empirical parameter $m = 15$ (appropriate for sandstone as a representative clast lithology), average overburden density $\rho = 2700$ kg m^{-3} and gravitational acceleration g (both failure criteria and rock properties detailed by Jaeger et al., 2007). For $f_p = 0.75$, as estimated for Nankai (Saffer and Tobin, 2011), $\tau_{max} = \tau_0 = 179$ MPa is required for clast shear fracture at 40 km depth and $\tau_0 = 268$ MPa for tensile fracture (larger than the predicted $\tau_0 \sim 10$ MPa). However,

considering clast stress amplification to $\tau_{max}/\tau_0 \approx 4.7$ when $\eta_m/\eta_c = 10^{-2}$ (taking the average of the model range; Fig. 3a), clast failure is consistent with a lower bulk mélange stress of $\tau_0 = 38$ MPa (shear failure) and $\tau_0 = 57$ MPa (tensile failure). Stress amplification is even greater with increased viscosity contrast, e.g. $\tau_{max}/\tau_0 \approx 10.1$ for $\eta_m/\eta_c = 10^{-4}$, reducing the bulk shear stress required for clast failure to $\tau_0 = 18$ MPa (shear) and $\tau_0 = 27$ MPa (tensile), approaching the estimated $\tau_0 \sim 10$ MPa without invoking near-lithostatic pore-pressure.

6. Stick-Slip Creep Behavior and Slow Slip Events

SSEs can be represented by slow stick-slip instabilities caused by competing weakening and strengthening rate-and-state mechanisms (Rubin, 2008), variation in pore-pressure (Bernaudin and Gueydan, 2018) or alternating clast-supported and matrix-supported bulk rheology (Lavier et al., 2013; Webber et al., 2018). Our mélange models undergoing progressive jamming demonstrate that the most generalized mélange can switch between matrix-support and clast-support, resulting in significant η_{eff} variation through time.

Prior to jamming, the model with $\phi = 0.64$ and $w = 2$ m has a relatively low $\eta_{eff}/\eta_m = 6.8$ (Fig. 2), consistent with η_{eff} inferred during SSEs. For example, using 50 cm yr^{-1}, equivalent to $\dot{\epsilon}_{xy} = 8 \times 10^{-11}$ s^{-1} for $w = 100$ m , and assuming $\tau_0 = 10$ MPa, the unjammed mélange must have $\eta_{eff} \approx 6 \times 10^{16}$ Pa s (following Eq. 1). Therefore $\eta_m = \eta_{eff}/6.8 = 9 \times 10^{15}$ Pa s, which is low, but could correspond to pressure-solution in fluid saturated conditions with fine grain size (Den Hartog and Spiers, 2014; Fagereng and den Hartog, 2017). Upon jamming, η_{eff} increases to $172\eta_m$. Jamming would lower the slip rate (which varies inversely proportionally to η_{eff}, assuming unchanged η_m, τ and w) to 2 cm yr^{-1}, slower than typical plate velocities. This could trigger the end of an SSE and the initiation of elastic strain accumulation. Generalized mélange within a relatively thick shear zone can therefore have jammed and unjammed states which may correspond to the periods between and during SSEs respectively. Jamming occurs in our models at a lower ϕ (≥ 0.5) than previous estimates ($\phi > 0.8$-0.9; Fagereng & Sibson, 2010; Grigull et al., 2012) and therefore may be more widespread than previously thought.

The SSE cycle also requires unjamming, which was not modelled. In experiments, stick-slip behavior is inferred to correspond to the periodic breaking and reorganization of force chains (Anthony and Marone, 2005). Fracturing of jammed clasts, caused by stress amplification, may reduce clast strength through velocity-weakening behavior and/or cohesion loss. Unstable rupture could be prevented by velocity-strengthening matrix slip as predicted for wet illite and quartz/illite gouges at SSE velocities and relevant temperatures (Den Hartog et al., 2014). Temporary deactivation of force chains would switch the mélange to matrix-supported deformation, dramatically reducing η_{eff} and potentially triggering an SSE. The period between SSEs may then depend on the healing time for clast fractures (e.g. Rubin, 2008). The jamming tendency of mélange provides potential for stick-slip behavior through distributed shear-zone deformation, though this must be tested using models with non-linear rheology.

Periodic jamming and unjamming of mélange with high ϕ may explain why there is a patch of relatively high interseismic coupling in the northern Hikurangi (near Gisborne, New Zealand), which slips aseismically during SSEs (Wallace & Beavan, 2010; Wallace et al., 2016). This patch, embedded in a region of low coupling, is thought to coincide with a region of decreased clay content and pore-pressure (Heise et al., 2017) and/or the presence of a rigid seamount updip of a highly over-pressured region (Bell et al., 2010). Thin or clay-poor shear zones may therefore be intermittently dominated by stronger block rheologies, while still participating in SSEs when force chains break.

7. Length Scale of Low Frequency Earthquakes

The rupture size of LFEs appears to be limited (Bostock et al., 2015), to ~ 100 m diameter patches (Chestler & Creager, 2017). The areas of individual force chains and length of high matrix strain-rate regions are finite in the mélange models and of similar scale in both 1 m and 2 m thick cases (Fig. 1). These cannot be upscaled using w, leaving L_{clast} as the relevant length scale. Force chains are generally limited by L_{clast}, transmitting stress through single large clasts and groups of smaller clasts (Fig. 1). If the largest magnitude LFEs correspond to fracture of the largest single blocks, these would need to have a cross-section length of ~ 100 m. Patches of locally elevated matrix strain-rate can reach $\sim 2\ L_{clast}$. A 100 m long localized region of high matrix strain-rate could then occur in matrix flowing around blocks with

$L_{clast} = 50$ m (short axis length of 17 m). Blocks of this scale exist in the Franciscan mélange (Grigull et al., 2012), though smaller blocks may also be suitable if that collectively act as one block, or the length-scale of localized matrix deformation is longer for a non-linear rheology or dynamic rupture. An active shear zone, typically 100 m thick, with blocks < 50 m long would have a similar L_{clast}/w ratio as the wide end-member model. Such a mélange only needs a small number of force chains spanning the shear zone to promote stick-slip behavior.

8. Conclusions

Generalized numerical models simulating viscous shear of subduction-style mélanges demonstrate that relatively rapid aseismic slip can be accommodated by distributed deformation, provided $\phi < 0.5$ or force chains are temporarily deactivated (e.g. due to clast failure). Mélange strength can dynamically increase > 10-fold as jamming occurs, supporting a hypothesis that the episodicity of SSEs is related to force chain dynamics within a heterogeneous shear zone. Creeping mélange with a low deviatoric stress can still generate high stresses within strong clasts and blocks, predicted to result in fracturing at < 40 km depth, even with only moderate pore-fluid overpressure. Such stress amplification reconciles fracturing of strong components with small observed stress drops. Tremor may correspond to fracturing of large blocks or localized slip of intervening matrix minerals, with length-scale of failure limited by the size of the largest mélange blocks, which itself is limited by shear zone width. Episodic slow slip and tremor may therefore be associated with mélange deformation at the 10 to 100 m scale, occurring in regions with dynamic block-scale force chains.

Acknowledgements

This project has received funding from the European Research Council (ERC) under the European Union's Horizon 2020 research and innovation programme (Starting Grant agreement No 715836 "MICA"). The ARCCA Raven computing cluster (Cardiff University) was used for all numerical calculations. Ellis was supported by MBIE Endeavour and core research funds to GNS Science. The open-source geodynamic code Underworld is available

at http://www.underworldcode.org and model parameters required to replicate the results are detailed in the manuscript. We thank the reviewers for their helpful comments.

References

Anthony, J. L., & Marone, C. (2005). Influence of particle characteristics on granular friction. *Journal of Geophysical Research: Solid Earth*, *110*(B8).

Bachmann, R., Oncken, O., Glodny, J., Seifert, W., Georgieva, V., & Sudo, M. (2009). Exposed plate interface in the European Alps reveals fabric styles and gradients related to an ancient seismogenic coupling zone. *Journal of Geophysical Research: Solid Earth*, *114*(5), 1–23. https://doi.org/10.1029/2008JB005927

Behr, W. M., Kotowski, A. J., & Ashley, K. T. (2018). Dehydration-induced rheological heterogeneity and the deep tremor source in warm subduction zones. *Geology*. https://doi.org/10.1130/G40105.1

Bell, R., Sutherland, R., Barker, D. H. N., Henrys, S., Bannister, S., Wallace, L., & Beavan, J. (2010). Seismic reflection character of the Hikurangi subduction interface, New Zealand, in the region of repeated Gisborne slow slip events. *Geophysical Journal International*, *180*(1), 34–48. https://doi.org/10.1111/j.1365-246X.2009.04401.x

Bernaudin, M., & Gueydan, F. (2018). Episodic tremor and slip explained by fluid-enhanced microfracturing and sealing. *Geophysical Research Letters*, *45*(8), 3471-3480.

Bos, B., Peach, C. J., & Spiers, C. J. (2000). Frictional-viscous flow of simulated fault gouge caused by the combined effects of phyllosilicates and pressure solution. *Tectonophysics*, *327*(3–4), 173–194. https://doi.org/10.1016/S0040-1951(00)00168-2

Byerlee, J. (1978). Friction of rocks. In *Rock friction and earthquake prediction* (pp. 615-626). Birkhäuser, Basel.

Byrne, T. and Fisher, D., 1990. Evidence for a weak and overpressured decollement beneath sediment-dominated accretionary prisms. *Journal of Geophysical Research: Solid Earth*, *95*(B6), pp.9081-9097.

Cates, M. E., Wittmer, J. P., Bouchaud, J. P., & Claudin, P. (1998). Jamming, force chains, and fragile matter. *Physical Review Letters*, *81*(9), 1841–1844. https://doi.org/10.1103/PhysRevLett.81.1841

Chestler, S. R., & Creager, K. C. (2017). Evidence for a scale-limited low-frequency earthquake source process. *Journal of Geophysical Research: Solid Earth*, *122*(4), 3099–3114. https://doi.org/10.1002/2016JB013717

Davis, D., Suppe, J., & Dahlen, F. (1983). Mechanisms of Fold-and-Thrust Belts and Accretionary Wedges. *Journal of Geophysical Research*, *88*(B2), 1153–1172.

Deubelbeiss, Y., & Kaus, B. J. P. (2008). Comparison of Eulerian and Lagrangian numerical techniques for the Stokes equations in the presence of strongly varying viscosity. *Physics of the Earth and Planetary Interiors*, *171*(1-4), 92-111.

Dimitrova, L. L., Wallace, L. M., Haines, A. J., & Williams, C. A. (2016). High-resolution view of active tectonic deformation along the Hikurangi subduction margin and the Taupo Volcanic Zone, New Zealand. *New Zealand Journal of Geology and Geophysics*, *59*(1), 43–57. https://doi.org/10.1080/00288306.2015.1127823

Dragert, H., Wang, K., & James, T. S. (2001). A silent slip event on the deeper Cascadia subduction interface. *Science*, *292*(5521), 1525–1528. https://doi.org/10.1126/science.1060152

Duarte, J. C., Schellart, W. P., & Cruden, A. R. (2015). How weak is the subduction zone interface? *Geophysical Research Letters*, *42*(8), 2664–2673. https://doi.org/10.1002/2014GL062876

Fagereng, Å. (2011a). Frequency-size distribution of competent lenses in a block-in-matrix mélange: Imposed length scales of brittle deformation? *Journal of Geophysical Research: Solid Earth*, *116*(5), 1–12. https://doi.org/10.1029/2010JB007775

Fagereng, Å. (2011b). Geology of the seismogenic subduction thrust interface. *Geological Society, London, Special Publications*, *359*(1), 55–76. https://doi.org/10.1144/SP359.4

Fagereng, Å., & Den Hartog, S. A. M. (2017). Subduction megathrust creep governed by pressure solution and frictional-viscous flow. *Nature Geoscience*, *10*(1), 51–57. https://doi.org/10.1038/ngeo2857

Fagereng, Å., & Sibson, R. H. (2010). Mélange rheology and seismic style. *Geology*, *38*(8), 751–754. https://doi.org/10.1130/G30868.1

Fagereng, Å., Remitti, F., & Sibson, R. H. (2011). Incrementally developed slickenfibers - Geological record of repeating low stress-drop seismic events? *Tectonophysics*, *510*(3–4), 381–386. https://doi.org/10.1016/j.tecto.2011.08.015

Fagereng, Å., Hillary, G. W. B., & Diener, J. F. A. (2014). Brittle-viscous deformation, slow slip, and tremor. *Geophysical Research Letters*, *41*(12), 4159–4167. https://doi.org/10.1002/2014GL060433

Fullsack, P. (1995). An arbitrary Lagrangian-Eulerian formulation for creeping flows and its application in tectonic models. *Geophysical Journal International*, *120*(1), 1-23.

Gao, X., & Wang, K. (2014). Strength of stick-slip and creeping subduction megathrusts from heat flow observations. *Science*, *345*(6200), 1038–1041. https://doi.org/10.1126/science.1255487

Grigull, S., Krohe, A., Moos, C., Wassmann, S., & Stöckhert, B. (2012). "Order from chaos": A field-based estimate on bulk rheology of tectonic mélanges formed in subduction zones. *Tectonophysics*, *568–569*, 86–101. https://doi.org/10.1016/j.tecto.2011.11.004

Handy, M. R. (1994). Flow laws for rocks containing two non-linear viscous phases: A phenomenological approach. *Journal of Structural Geology*, *16*(3), 287–301. https://doi.org/10.1016/0191-8141(94)90035-3

Den Hartog, S. A. M., & Spiers, C. J. (2014). A microphysical model for fault gouge friction applied to subduction megathrusts. *Journal of Geophysical Research: Solid Earth*, *119*(2), 1510–1529. https://doi.org/10.1002/2013JB010580

Den Hartog, S., Saffer, D. M., & Spiers, C. J. (2014). The roles of quartz and water in controlling unstable slip in phyllosilicate-rich megathrust fault gouges. *Earth, Planets and Space*, *66*(78), 1–9. https://doi.org/10.1186/1880-5981-66-78

Hawthorne, J. C., & Rubin, A. M. (2010). Tidal modulation of slow slip in Cascadia. *Journal of Geophysical Research: Solid Earth*, *115*(B9).

Hayman, N. W., & Lavier, L. L. (2014). The geologic record of deep episodic tremor and slip. *Geology*, *42*(3), 195–198. https://doi.org/10.1130/G34990.1

Heise, W., Caldwell, T. G., Bannister, S., Bertrand, E. A., Ogawa, Y., Bennie, S. L., & Ichihara, H. (2017). Mapping subduction interface coupling using magnetotellurics: Hikurangi margin, New Zealand. *Geophysical Research Letters*, *44*(18), 9261–9266. https://doi.org/10.1002/2017GL074641

Hilairet, N., Reynard, B., Wang, Y., Daniel, I., Merkel, S., Nishiyama, N., & Petitgirard, S. (2007). High-pressure creep of serpentine, interseismic deformation, and initiation of subduction. *Science*, *318*(5858), 1910-1913.

Ide, S., Beroza, G. C., Shelly, D. R., & Uchide, T. (2007a). A scaling law for slow earthquakes. *Nature*, *447*(7140), 76–79. https://doi.org/10.1038/nature05780

Ide, S., Shelly, D. R., & Beroza, G. C. (2007b). Mechanism of deep low frequency earthquakes: Further evidence that deep non-volcanic tremor is generated by shear slip on the plate interface. *Geophysical Research Letters*, *34*(3). https://doi.org/10.1029/2006GL028890

Jaeger, J. C., Cook, N. G., & Zimmerman, R. (2009). *Fundamentals of rock mechanics.* John Wiley & Sons.

Ji, S. (2004). A generalized mixture rule for estimating the viscosity of solid-liquid suspensions and mechanical properties of polyphase rocks and composite materials. *Journal of Geophysical Research: Solid Earth*, *109*(10), 1–18. https://doi.org/10.1029/2004JB003124

Kano, M., Kato, A., Ando, R., & Obara, K. (2018). Strength of tremor patches along deep transition zone of a megathrust. *Scientific reports*, *8*(1), 3655.

Krieger, I. M., & Dougherty, T. J. (1959). A Mechanism for Non-Newtonian Flow in Suspensions of Rigid Spheres. *Transactions of the Society of Rheology*, *3*(1), 137–152. https://doi.org/10.1122/1.548848

Lavier, L. L., Bennett, R. A., & Duddu, R. (2013). Creep events at the brittle ductile transition. *Geochemistry, Geophysics, Geosystems*, *14*(9), 3334–3351. https://doi.org/10.1002/ggge.20178

Luo, Y., & Ampuero, J. P. (2017). Stability of faults with heterogeneous friction properties and effective normal stress. *Tectonophysics*, (November), 1–16. https://doi.org/10.1016/j.tecto.2017.11.006

Miyazaki, S., Segall, P., McGuire, J. J., Kato, T., & Hatanaka, Y. (2006). Spatial and temporal evolution of stress and slip rate during the 2000 Tokai slow earthquake. *Journal of Geophysical Research: Solid Earth*, *111*(3), 1–17. https://doi.org/10.1029/2004JB003426

Moresi, L., Quenette, S., Lemiale, V., Mériaux, C., Appelbe, B., & Mühlhaus, H. B. (2007). Computational approaches to studying non-linear dynamics of the crust and mantle. *Physics of the Earth and Planetary Interiors*, *163*(1–4), 69–82. https://doi.org/10.1016/j.pepi.2007.06.009

Nakata, R., Suda, N., & Tsuruoka, H. (2008). Non-volcanic tremor resulting from the combined effect of Earth tides and slow slip events. *Nature Geoscience*, *1*(10), 676–678. https://doi.org/10.1038/ngeo288

Niemeijer, A. R., & Spiers, C. J. (2007). A microphysical model for strong velocity weakening in phyllosilicate-bearing fault gouges. *Journal of Geophysical Research: Solid Earth*, *112*(10), 1–12. https://doi.org/10.1029/2007JB005008

Obara, K., Hirose, H., Yamamizu, F., & Kasahara, K. (2004). Episodic slow slip events accompanied by non-volcanic tremors in southwest Japan subduction zone. *Geophysical Research Letters*, *31*(23), 1–4. https://doi.org/10.1029/2004GL020848

Richardson, R. M., & Coblentz, D. D. (1994). Stress modeling in the Andes: Constraints on the South American intraplate stress magnitudes. *Journal of Geophysical Research: Solid Earth*, *99*(B11), 22015–22025. https://doi.org/10.1029/94JB01751

Rogers, G., & Dragert, H. (2003). Episodic tremor and slip on the Cascadia subduction zone: the chatter of silent slip. *Science (New York, N.Y.)*, *300*(5627), 1942–3. https://doi.org/10.1126/science.1084783

Roscoe, R. (1952). The viscosity of suspension of rigid spheres. *British Journal of Applied Physics*, *3*(AUG), 267–269.

Rowe, C. D., Moore, J. C., & Remitti, F. (2013). The thickness of subduction plate boundary faults from the seafloor into the seismogenic zone. *Geology*, *41*(9), 991–994. https://doi.org/10.1130/G34556.1

Rubin, A. M. (2008). Episodic slow slip events and rate-and-state friction. *Journal of Geophysical Research: Solid Earth*, *113*(B11).

Rubinstein, J. L., La Rocca, M., Vidale, J. E., Creager, K. C., & Wech, A. G. (2008). Tidal modulation of nonvolcanic tremor. *Science, 319*(5860), 186-189.

Rybacki, E., Gottschalk, M., Wirth, R., & Dresen, G. (2006). Influence of water fugacity and activation volume on the flow properties of fine-grained anorthite aggregates. *Journal of Geophysical Research: Solid Earth*, *111*(B3).

Saffer, D. M., & Marone, C. (2003). Comparison of smectite-and illite-rich gouge frictional properties: application to the updip limit of the seismogenic zone along subduction megathrusts. *Earth and Planetary Science Letters*, *215*(1-2), 219-235.

Saffer, D. M., & Tobin, H. J. (2011). Hydrogeology and mechanics of subduction zone forearcs: Fluid flow and pore pressure. *Annual Review of Earth and Planetary Sciences, 39*, 157-186.

Schmid, D. W., & Podladchikov, Y. Y. (2003). Analytical solutions for deformable elliptical inclusions in general shear. *Geophysical Journal International*, *155*(1), 269–288. https://doi.org/10.1046/j.1365-246X.2003.02042.x

Schwartz, S. Y., & Rokosky, J. M. (2007). Slow slip events and seismic tremor at circum-Pacific subduction zones. *Reviews of Geophysics*, *45*(3), n/a-n/a. https://doi.org/10.1029/2006RG000208

Shreve, R. L., & Cloos, M. (1986). Dynamics of sediment subduction, melange formation, and prism accretion. *Journal of Geophysical Research*, *91*(B10), 10229. https://doi.org/10.1029/JB091iB10p10229

Sibson, R. H. (2013). Stress switching in subduction forearcs: Implications for overpressure

containment and strength cycling on megathrusts. *Tectonophysics*, *600*, 142–152. https://doi.org/10.1016/j.tecto.2013.02.035

Sibson, R. H. (2014). Earthquake rupturing in fluid-overpressured crust: how common? *Pure and Applied Geophysics, 171*(11), 2867-2885.

Treagus, S. H. (2002). Modelling the bulk viscosity of two-phase mixtures in terms of clast shape. *Journal of Structural Geology*, *24*(1), 57–76. https://doi.org/10.1016/S0191-8141(01)00049-9

Ujiie, K., Saishu, H., Fagereng, Å., Nishiyama, N., Otsubo, M., Masuyama, H. and Kagi, H., 2018. An explanation of episodic tremor and slow slip constrained by crack-seal veins and viscous shear in subduction mélange. *Geophysical Research Letters.*

Wallace, L. M., & Beavan, J. (2010). Diverse slow slip behavior at the Hikurangi subduction margin, New Zealand. *Journal of Geophysical Research: Solid Earth*, *115*(12), 1–20. https://doi.org/10.1029/2010JB007717

Wallace, L. M., Webb, S. C., Ito, Y., Mochizuki, K., Hino, R., Henrys, S., ... & Sheehan, A. F. (2016). Slow slip near the trench at the Hikurangi subduction zone, New Zealand. *Science, 352*(6286), 701-704.

Webber, S., Ellis, S., & Fagereng, Å. (2018). "Virtual shear box" experiments of stress and slip cycling within a subduction interface mélange. *Earth and Planetary Science Letters*, *488*, 27–35. https://doi.org/10.1016/j.epsl.2018.01.035

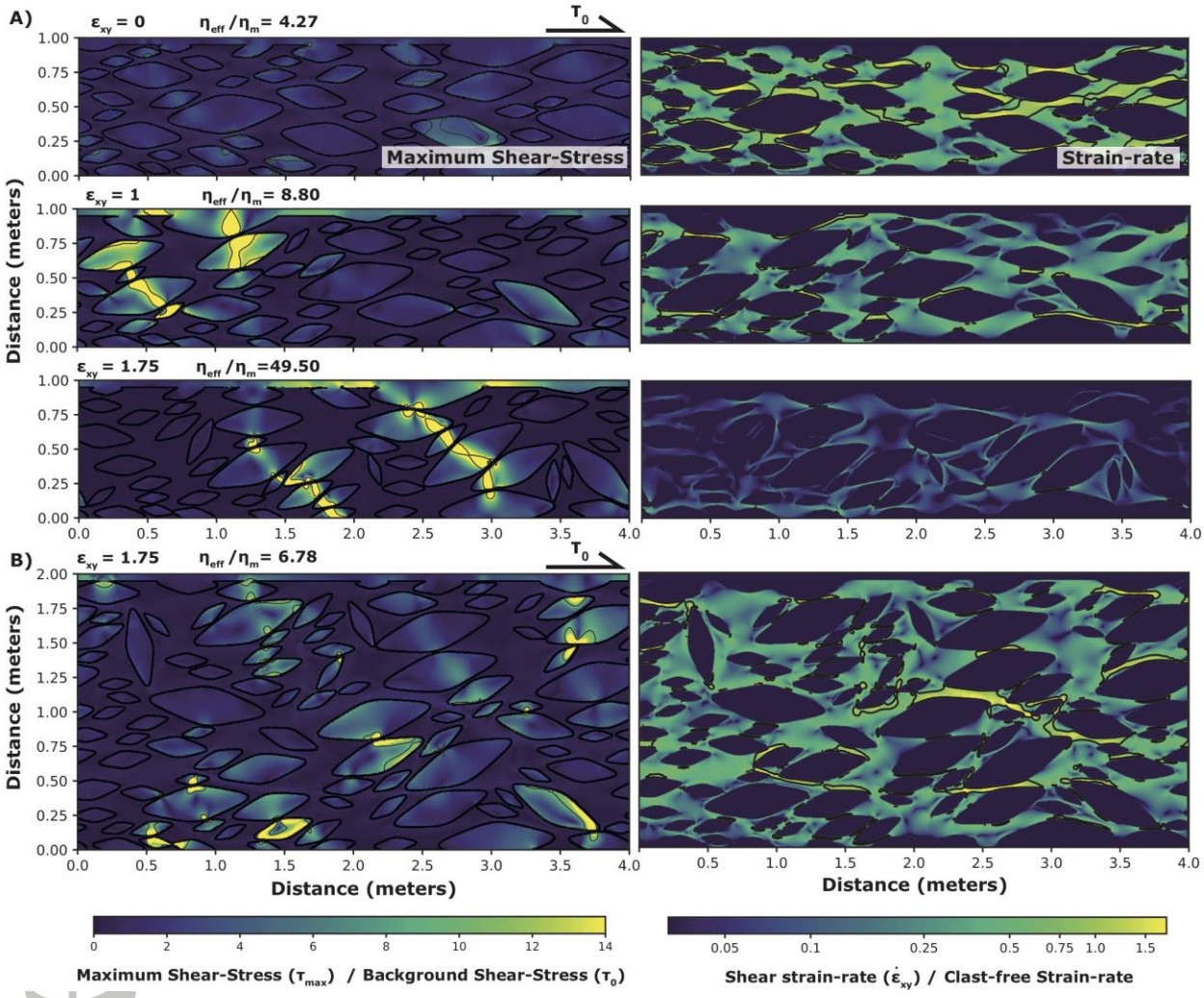

Figure 1. Model evolution for $\phi = 0.5$ and $\eta_m/\eta_c = 10^{-4}$, showing maximum shear-stress (clasts outlined, contours drawn for the 95th percentile τ_{95}) and shear-zone-parallel shear strain-rate (each scale capped for visualization). Strain-rate is normalized against a 'clast-free' strain-rate corresponding to a model with $\phi = 0$ (contours drawn for 75% of the clast-free strain-rate). (a) Progressively strained 1 m thick model, with increased occurrence of force chains (adjacent clasts with high τ_{max}) at high strain and subsequent jamming (increase in η_{eff}/η_m). Prior to jamming, localized matrix regions of high strain-rate occur at the edges of clasts involved in force chains. (b) 2 m thick model. Force chains occur, but without spanning the model thickness, preventing jamming.

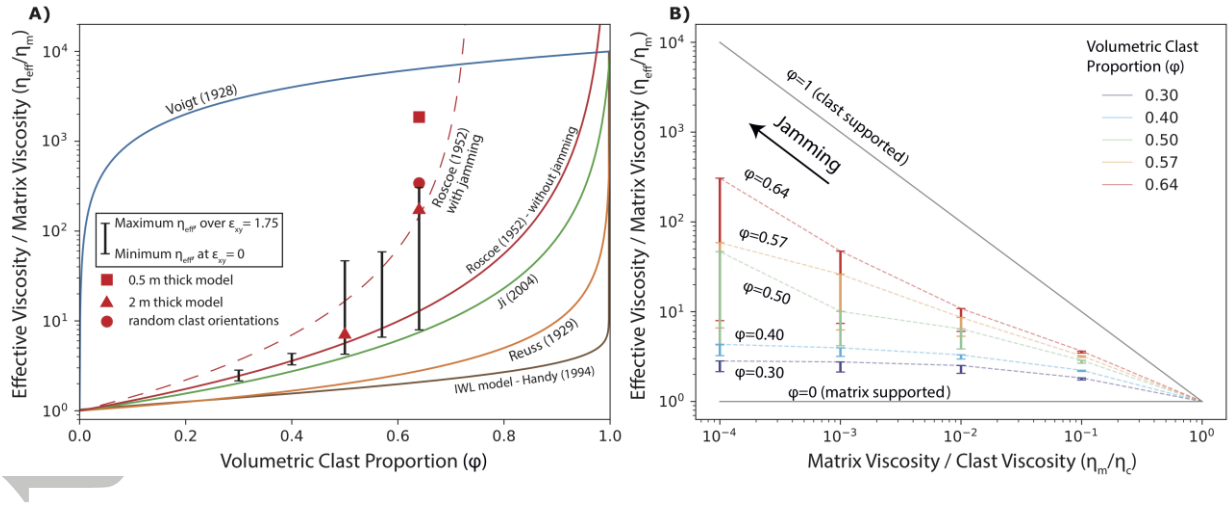

Figure 2. Minimum and maximum bulk viscosities (lower and upper brackets) of the 'reference' models ($w = 1$ m), as a function of ϕ (a) Models with $\eta_m/\eta_c = 10^{-4}$, compared to typically used mixture laws (Handy, 2004; Ji, 2004; Roscoe, 1952; Reuss and Voigt end-member models). At zero strain, η_{eff} is well described by the Roscoe and Ji models. At high strain and $\phi \geq 0.5$, η_{eff} increases significantly and is better approximated by models incorporating jamming (dashed line). The maximum η_{eff} of the 'additional' models with varying fault zone thickness and initial clast orientations are also shown (red symbols). (b) Models with both varying ϕ and η_m/η_c. Models with $\phi \geq 0.5$ move towards a clast-supported trend for $\eta_m/\eta_c \leq 10^{-3}$ (horizontal grey line).

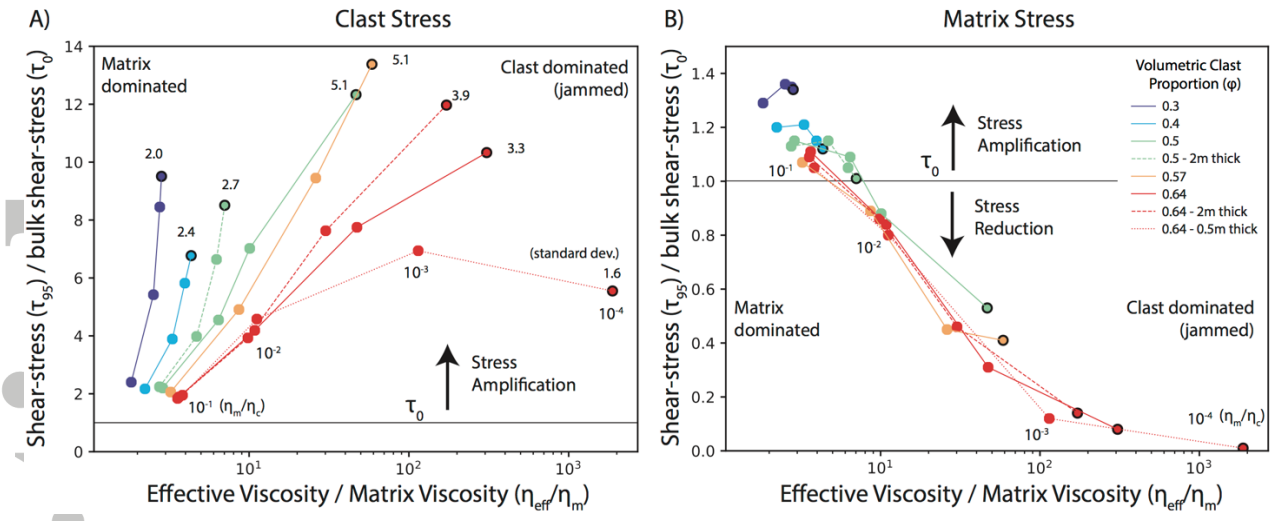

Figure 3. Measures of stress variation within the model domain, as a function of jamming (quantified as η_{eff}/η_m) and plotted for a range of ϕ (colors) and η_m/η_c (successive points labelled, with the weakest model emphasized). (a) The highest clast stress amplification (τ_{95}) occurs at moderate jamming ($30 \leq \eta_{eff}/\eta_m \leq 100$). Relatively high stress amplification of ≤ 9.5x still occurs for little jamming ($\eta_{eff}/\eta_m < 10$). Figures above each curve give standard deviation of τ_{max} over the whole domain. (b) The highest matrix shear stress (τ_{95}) decreases with increasing jamming, eventually reducing to below the background stress.